Synaptic Plasticity in the Medial Superior Olive of Hearing, Deaf, and Cochlear-Implanted Cats

Natasha N. Tirko[1] and David K. Ryugo[2,3,4]*

[1]Department of Biomedical Engineering, Center for Hearing and Balance, Johns Hopkins University School of Medicine, Baltimore, Maryland 21205, USA
[2]Department of Neuroscience, Center for Hearing and Balance, Johns Hopkins University School of Medicine, Baltimore, Maryland 21205, USA
[3]Department of Otolaryngology, Center for Hearing and Balance, Johns Hopkins University School of Medicine, Baltimore, Maryland 21205, USA
[4]Garvan Institute of Medical Research, Darlinghurst, NSW 2010, Australia

ABSTRACT

The medial superior olive (MSO) is a key auditory brainstem structure that receives binaural inputs and is implicated in processing interaural time disparities used for sound localization. The deaf white cat, a proven model of congenital deafness, was used to examine how deafness and cochlear implantation affected the synaptic organization at this binaural center in the ascending auditory pathway. The patterns of axosomatic and axodendritic organization were determined for principal neurons from the MSO of hearing, deaf, and deaf cats with cochlear implants. The nature of the synapses was evaluated through electron microscopy, ultrastructure analysis of the synaptic vesicles, and immunohistochemistry. The results show that the proportion of inhibitory axosomatic terminals was significantly smaller in deaf animals when compared with hearing animals. However, after a period of electrical stimulation via cochlear implants the proportion of inhibitory inputs resembled that of hearing animals. Additionally, the excitatory axodendritic boutons of hearing cats were found to be significantly larger than those of deaf cats. Boutons of stimulated cats were significantly larger than the boutons in deaf cats, although not as large as in the hearing cats, indicating a partial recovery of excitatory inputs to MSO dendrites after stimulation. These results exemplify dynamic plasticity in the auditory brainstem and reveal that electrical stimulation through cochlear implants has a restorative effect on synaptic organization in the MSO. J. Comp. Neurol. 520:2202–2217, 2012.

INDEXING TERMS: synaptic excitation and inhibition; synaptic vesicles; congenital deafness; cochlear implant stimulation

The medial superior olive (MSO) is considered a "coincidence detector," and is traditionally implicated in the processing of interaural time differences (ITDs) used for low-frequency sound localization. The principal neurons of the MSO, whose cell bodies are aligned in an elongated column with two bilaterally extending dendrites (Scheibel and Scheibel, 1974; Kulesza, 2007), receive bilateral excitatory inputs from the spherical bushy cells of the anteroventral cochlear nucleus (AVCN) (Jeffress, 1948; Stotler, 1953; Cant and Hyson, 1992; Smith et al., 1993; Grothe, 1994), a population of cochlear nucleus neurons that are superb in preserving timing features of acoustic stimuli (Bourk, 1976; Smith et al., 1993; Babalian et al., 2003). Consequently, MSO cells are well situated to compare the timing of both ipsi- and contralateral excitatory inputs. The MSO cell bodies receive inhibitory input from the medial and lateral nuclei of the trapezoid body (MNTB, LNTB), which integrates with the dendritic excitation to provide ITD sensitivity to ≈10 μsec (Clark, 1969; Cant and Morest, 1984; Cant and Hyson, 1992; Kapfer et al., 2002).

Studies on the development of the MSO have shown spatial refinement of synaptic inputs over time. Data from

Grant sponsor: National Institutes of Health (NIH); Grant number: DC000232; Grant sponsor: Advanced Bionics, and a Life Sciences Research Award from the Office for Science and Medical Research, NSW.

*CORRESPONDENCE TO: David K. Ryugo, Garvan Institute, 384 Victoria St., Darlinghurst, NSW 2010 Australia. E-mail: d.ryugo@garvan.org.au

Received July 28, 2011; Revised November 14, 2011; Accepted January 7, 2012
DOI 10.1002/cne.23038
Published online January 11, 2012 in Wiley Online Library (wileyonlinelibrary.com)

gerbil brainstem slices have shown that the effect of gamma-aminobutyric acid (GABA)(B) receptors in young animals is stronger for excitatory compared with inhibitory transmission in the MSO principal cells, but that in mature animals GABA(B) receptors mainly control inhibition. During this same developmental period there is a shift in location of these receptors from dendrites to cell body (Hassfurth et al., 2010). This refinement fails to develop in mammals that do not use ITDs for sound localization and is experience-dependent; deafness disrupts these spatially segregated excitatory and inhibitory input patterns (Kapfer et al., 2002). Because deafness results in definable abnormalities in structure and function throughout the central auditory system (West and Harrison, 1973; Schwartz and Higa, 1982; Ryugo et al., 1997, 1998; Heid et al., 1998; Kral et al., 2002, 2005), one question is to what extent the pathology can be reversed by the introduction of auditory stimulation.

The restorative effects of early electrical stimulation via cochlear implantation have been reported in a number of locations in the central auditory pathway including the cochlear nucleus (Matsushima et al., 1991; Lustig et al., 1994; Chao et al., 2002; Ryugo et al., 2005; O'Neil et al., 2010) and cerebral cortex (Klinke et al., 1999). However, the effects of cochlear implant stimulation on the anatomy and physiology of the MSO have not been previously investigated. There is a need to understand the structural and functional changes in the MSO after cochlear stimulation because of growing acceptance for both unilateral and bilateral cochlear implantation in humans. Studies report that bilateral implant users gain advantages in speech perception (Dunn et al., 2006) but their ability to process ITDs is relatively poor compared with normal hearing listeners (van Hoesel, 2004, 2007). Ironically, ITDs provide the greatest binaural benefits with low-frequency sounds in normal listeners, so it is of significant relevance to assess the plastic response of MSO neurons to restored hearing. In theory, bilateral cochlear implants should enrich the acoustic experience by providing cues that contribute to sound localization. Better sound localization skills should then improve signal discrimination in noise, enhance sound quality, and foster better speech understanding.

We studied the synaptic organization of three cohorts of cats: hearing, congenitally deaf, and congenitally deaf with cochlear implants. Congenital deafness in the white cat (DWC) is correlated with the collapse of Reissner's membrane onto the organ of Corti that commences during the second week of life (Mair, 1973). This pathology is accompanied by a thinning of the stria vascularis and a malformation of the tectorial membrane (Ryugo et al., 2003). The spiral ganglion cells exhibit smaller cell bodies and gradually decline in number to ≈40% of their original population size by the end of the first postnatal year (Chen et al., 2010). The inner ear pathology of these cats resembles that of the Scheibe-type deformity of cochleosaccular degeneration found in human hereditary deafness (Elverland and Mair, 1980), making it an attractive model for a study of cochlear implant stimulation.

The ultrastructure of the MSO was assessed using a novel, quantitative method to analyze synaptic vesicle (SV) shape and size. Fine structural analysis via electron microscopy has proven to be the benchmark for describing synapse morphology, plasticity, and function (Peters et al., 1991; Schikorski and Stevens, 1997; Petralia et al., 2003; Matthews and Sterling, 2008). We also applied immunohistochemical methods to confirm the validity of the SV analysis, further supporting our use of SV shape as an indication of synaptic behavior. Combining these methods revealed remarkable synaptic plasticity in the MSO as a result of cochlear implant stimulation.

MATERIALS AND METHODS

Animals

The MSOs of 17 cats were used in the electron microscopy analysis: adult hearing ($n = 5$), adult deaf ($n = 5$), unilaterally cochlear implanted ($n = 3$), bilaterally cochlear implanted ($n = 2$), 90-day-old hearing ($n = 1$), and 90-day-old deaf ($n = 1$). An additional 10 cats were used for immunohistochemical analysis: adult hearing ($n = 3$), adult deaf ($n = 2$), and bilaterally cochlear implanted ($n = 5$). Hearing cats were pigmented, whereas the deaf and cochlear-implanted cats were nonpigmented. Some of these cats have contributed unrelated data to other studies (Kretzmer et al., 2004; Ryugo et al., 2005; O'Neil et al., 2010; Chen et al., 2010). All procedures were conducted in accordance with National Institutes of Health (NIH) guidelines and approved by the Johns Hopkins University Animal Care and Use Committee.

Hearing status assessment

The hearing status of all experimental cats was assessed by auditory brainstem responses (ABRs), because not all white cats are born deaf. Briefly, at age 30 days kittens were anesthetized (0.5 mg/kg xylazine and 0.1–0.24 mg/kg ketamine hydrochloride, intraperitoneally [IP]), had recording electrodes inserted caudal and rostral to the pinna on both sides, and had a grounding electrode placed in the neck. Clicks (100 μsec duration and alternating polarity) were presented at increasing intensities through a free-field speaker and evoked responses were averaged over 1,000 stimulus presentations. Animals were classified as hearing by the presence of normal ABR thresholds or deaf due to an absence of detectable ABRs to 95 dB SPL stimulation. The maximum

output of the speaker was ≈100 dB SPL (re 0.0002 dynes/cm^2) as measured using 16 kHz tone pips and a calibrated microphone placed in at the position of the ear. Protocols for ABR recording and threshold measurements (e.g., Ryugo et al., 1997, 2003; O'Neil et al., 2010) were implemented using MatLab (MathWorks, Natick, MA) on Tucker-Davis hardware (Alachua, FL).

Cochlear prosthesis and stimulation

Deaf kittens were surgically fitted with 6-electrode cochlear implants modified for use in kittens, containing a Clarion II type receiver with a custom electrode array (Advanced Bionics, Sylomar, CA). Unilaterally implanted animals (CIK) had electrode arrays placed in the left cochlea only, whereas bilaterally implanted animals (BCIK) had arrays placed in each cochlea. Radiograph analysis confirmed that the 6-mm electrode array was properly located, extending along the basal quarter of the cochlea, which is sensitive to frequencies of 13 kHz and higher (Liberman, 1982).

The bilateral cochlear implants consisted of symmetrical electrode arrays but only a single processor. Due to the small size of the kitten's head and the relatively large size of the processor, space was conserved by simplifying the implantable device. As a result, a single processor delivered identical impulses to each electrode array; there were no interaural delays. Because of this we analyzed the MSO of bilaterally stimulated cats using the same methodology as used when analyzing unilaterally stimulated cats. Conclusions concerning MSO synaptic plasticity differences between unilateral and bilateral stimulation is left to future studies, and will require integration of ITDs into the stimulation paradigm.

After a 10–14-day period of postsurgical recovery, functional electrodes with low impedance values were identified by behavioral cues (e.g., pupil dilation, pinna flicks, or vocalizations). Electrically evoked compound action potentials were also recorded in response to electrode activation. At least two functional electrodes were activated in each cat's stimulation program. Stimulation strength was optimized by selecting levels below that required to elicit motor responses. A microphone detected environmental and speech sounds in the laboratory, which were translated by a speech processor (Advanced Bionics) into biphasic electrical impulses and delivered to each electrode in the cochlea. The stimulation paradigm was a modification of the continuous interleaved sampling strategy, with >3,000 Hz carrier rate, biphasic pulses (21.6 μsec/phase). The pulses were amplitude-modulated by bandpass-filtered speaker output and distributed across the active electrodes (Advanced Bionics, HiRes cochlear implant). Electrodes were activated in a monopolar configuration.

The animals were acoustically stimulated for ≈3 months by voice, radio, and other ambient laboratory sounds for 7 hours per day, 5 days a week (O'Neil et al., 2010). Cats learned to approach their food bowl for a special treat (e.g., fresh roast beef, tuna, or canned sardines) in response to the invariant pairing to a specific bugle call. The behavioral shaping verified that implanted cats were processing and distinguishing physiologically relevant sounds. Because a monotonic version of the reinforced bugle call failed to elicit the approach behavior, it was evident that frequency was also an important and discriminable component of the stimulus.

Tissue preparation

At the end of the stimulation phase of the experiment, each animal was administered a lethal dose of sodium pentobarbital (75 mg/kg, IP) and perfused through the heart with a phosphate-buffered solution of 2% paraformaldehyde/2% glutaraldehyde, or 4% paraformaldehyde/0.1% glutaraldehyde. After overnight postfixation in the same solution, the brainstem was dissected and embedded in a gelatin-albumin mixture hardened with glutaraldehyde. Brainstem tissue samples were harvested from each animal using standard histological processing procedures for light and electron microscopy.

The brainstem tissue block was sectioned in the coronal plane (50–75 μm thickness) on a vibrating microtome. Sections were collected in serial order and separated into two series: one for light microscopy and immunohistochemistry, and one for electron microscopy. Those sections for electron microscopic analysis were placed in 1% OsO_4 for 15 minutes, rinsed in buffer, block stained in 1% uranyl acetate, rinsed, dehydrated, and embedded in PolyBed 812 between two sheets of Aclar.

Analysis was limited to the left medial superior olive and to the dendrites that were directed toward the left cochlear nucleus. This strategy meant that the output of the cochlear implant electrodes on the left side affected the dendrites under study by way of the ipsilateral cochlear nucleus (Stotler, 1953; Cant and Casseday, 1986). Analyses of the right-facing dendrites of the left MSO and of the dendrites of the contralateral MSO will be addressed in future studies. Pieces of the left MSO were isolated and the ventral third of the nucleus cut out and reembedded in BEEM capsules. This region of the MSO represents the high frequency response area (Guinan et al., 1972; Barrett, 1976; Grothe, 2000) and should have been preferentially activated by the cochlear implant stimulation. Ultrathin sections were collected on Formvar-coated slotted grids and examined with an electron microscope. Digital electron micrographs of MSO cell bodies, dendrites, and their associated synaptic endings were captured using a Hitachi H-7600 electron

microscope (Hitachi High-Tech, Tokyo, Japan) at 60 kV and 4,000× magnification for orientation purposes and 15,000–30,000× magnification for analysis.

Synaptic vesicle analysis

Digital electron micrographs were acquired for every visible synaptic ending on each MSO cell body in a given section. Cross-section location was consistently selected to be through the central region of the soma, as identified by the presence of the nucleus and nucleolus. Each image was imported into Adobe Photoshop CS3 (San Jose, CA) and contrast and brightness adjustments were made to improve clarity. Using a Cintiq Drawing Tablet (Wacom, Tokyo, Japan), outlines of all visible SVs within a synapse were drawn under 200% digital magnification. This process was completed for all synaptic endings on the cell soma included in the analysis by an analyzer blinded to the hearing status of the animals. The outlines were recorded as binary tiff images, which were then exported to MatLab for quantification of the SV attributes. A customized MatLab program analyzed the SV outlines and calculated the area and roundness values for every SV. Roundness was determined by approximating a best-fit ellipse to each outline. The ratio of the minor axis length to the major axis length was then called the roundness, with a value of one implying that an SV was perfectly circular.

Determination of SV type was completed using a graphical analysis method. Each SV measurement for a given synaptic ending was sorted into subgroups according to the vesicle area—100 nm^2 divisions ranging from 500 to 3,500 nm^2—and a mean roundness value was calculated for the subgroup. The resulting data were used to generate two plots: a scatter plot of the mean roundness of all vesicles in each subgroup and a line plot of the number of SVs within each subgroup. This method provided a quantitative graphical presentation of the shape and size distribution of all the SVs in every synapse.

The plots yield a clear separation of endings into two groups, distinguished by average roundness values. Terminals with pleomorphic SVs were identified as the group with lower roundness means, whereas endings with round SVs were grouped with higher roundness means. An additional grouping was observed within the endings having high roundness values; SV size separated into groups having small and large areas. A graph generated using this method of analysis shows small round, large round, and pleomorphic SV data (Fig. 1). These groups were confirmed as different for all MSO somata included in the analysis ($P < 0.05$, one-way Student's *t*-test). Additionally, outlines of MSO cell bodies containing a visible nucleolus were drawn, measured, and analyzed with respect to cross-sectional area and perimeter.

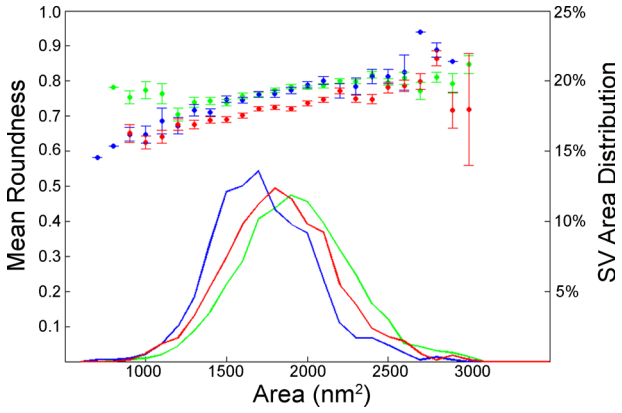

Figure 1. Graphical analysis of SVs with respect to size (area) and roundness differentiate between three different vesicle types: large round (green), small round (blue), and pleomorphic (red). The left y-axis corresponds to the scatterplot and shows the mean roundness for SVs (error bars show standard deviation) for each area bin. The line plots show the percent of SVs with respect to each area division as indicated by the right y-axis. The figure shows the averaged data of all somatic endings on one representative MSO cell. Large round and small round SVs have statistically similar roundness values, but small round vesicles have significantly smaller mean areas. Pleomorphic SVs have a significantly smaller mean roundness compared with that of round SVs.

Antibody characterization and immunohistochemistry

The anti-vesicular glutamate transporter 1 monoclonal antibody (mouse anti-VGLUT1, Chemicon MAB5502; Millipore, Billerica, MA) provided a pattern of cell morphology and distribution that was wholly consistent with previous publications using other antisera against VGLUT1 (e.g., Zhou et al., 2007). The anti-glycine transporter 2 neuronal polyclonal antibody (GlyT2, Chemicon AB1771; Millipore) yielded immunolabeling that mimicked the cellular morphology and distribution as previously published (Friauf et al., 1999; Zeilhofer et al., 2005). Specific details for these antibodies are provided in Table 1.

The patterns of glutamatergic and glycinergic synapses around MSO cell bodies were determined using standard immunocytochemical methods. Briefly, free-floating sections were blocked at room temperature in 10% normal goat serum for 1 hour, incubated overnight in mouse anti-VGLUT1 (1:1,000) or sheep anti-GlyT2 (1:1,000), washed, then incubated in appropriate biotinylated secondary antibody (1:200; Vector Labs, Burlingame, CA) for 2 hours, and treated with avidin-biotin complex (ABC Elite, Vector Labs) for 1 hour. Immunoreactions were visualized with 3,3′-diaminobenzidine (DAB, Sigma Chemical, St. Louis, MO). Tissue was then prepared for electron microscopy and subjected to the same SV analytical methods as described above.

TABLE 1.
Primary Antibodies for Immunohistochemistry

Antigen	Immunogen	Manufacturer details	Dilution used
Vesicular glutamate 1 transporter (VGLUT1)	Recombinant protein from rat VGLUT1	Chemicon MAB5502, mouse monoclonal	1:1,000
Vesicular glycine 2 transporter (GlyT2)	Synthetic peptide from C-terminus as predicted from cloned rat GlyT2	Chemicon AB1771, sheep polyclonal	1:1,000

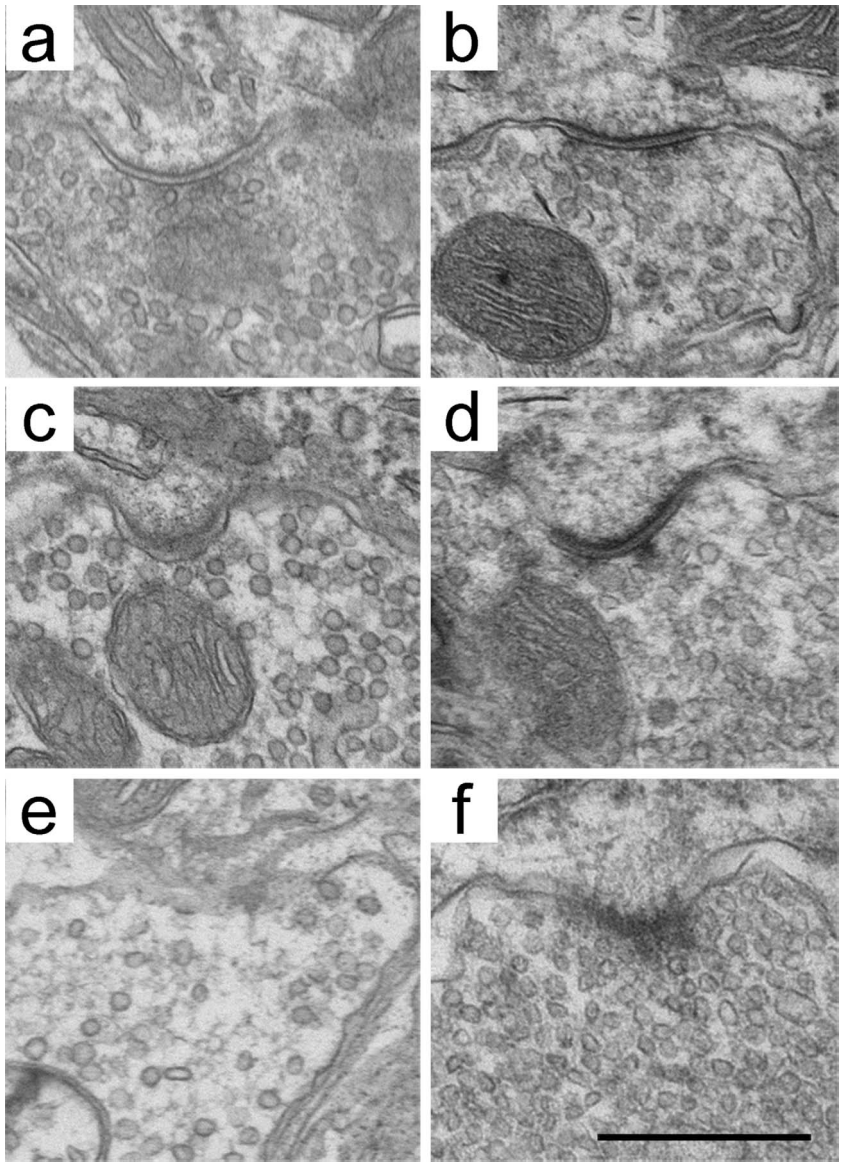

Figure 2. Three discrete SV types can be distinguished in each animal, regardless of variations due to fixation methods. Fixation with solutions containing 2% glutaraldehyde/2% paraformaldehyde (**a,c,e**) yields a more regular appearance of SV shape compared with that by fixation with 4% paraformaldehyde/0.1% glutaraldehyde (**b,d,f**). Regardless, pleomorphic (a,b), large round (c,d), and small round (e,f) SVs can still be distinguished within the same animal after quantifying area and roundness. Scale bar = 500 nm.

Axodendritic synapse analysis

All slides stained with VGLUT1 from adult hearing, deaf, and BCIK cats were numbered, coded, and put in random order into a microscope slide box. Bouton endings revealed by the BDA-DAB reaction product appeared as distinct oval structures that were found along the edge

of dendritic and somatic profiles. When observed through a light microscope, their presence along dendrites had the appearance of aphids on a stem.

Photomicrographs of the stained tissue through the left side of the medial superior olive were collected using a Jenoptik ProgRes C5 digital camera (Jena, Germany), a Zeiss Axioskop microscope, and a 100× oil immersion objective (NA 1.3). Images were selected to maximize the number of boutons in focus. The images were then traced using an interactive Cintiq graphics tablet, saved as a tiff file, and analyzed using ImageJ (NIH v1.44o). Area and roundness measurements were recorded.

Axodendritic synaptic contacts were also subjected to synaptic vesicle characterization, using similar methods to those used in axosomatic analyses. Terminals found on the left dendrites (ipsilateral to cochlear implants) of MSO principal cells were identified in electron micrographs and SV size and shape were quantified. Tissue sections containing dendritic processes from hearing ($n = 7$), deaf ($n = 6$), and unilateral cochlear-implanted ($n = 6$) cats were analyzed and the proportion of inhibitory terminals containing pleomorphic SVs was recorded. An average of 20 terminals were quantified in each tissue section.

RESULTS

Identification of synaptic vesicles

Three synaptic ending types were discernable by characterizing the SVs each contained: large round, small round, or pleomorphic (Fig. 2). While tissue fixed with 4% paraformaldehyde/0.1% glutaraldehyde had SVs with smaller roundness values than tissue fixed with 2% paraformaldehyde/2% glutaraldehyde, the within-animal comparisons of terminals with respect to roundness and size yielded a statistically significant division of three SV types. Endings with large and small round SVs had asymmetric postsynaptic densities (PSDs), which are associated with excitatory synapses, whereas endings with pleomorphic SVs had symmetric PSDs and are associated with inhibitory synapses (Uchizono, 1965). These relationships were confirmed by subsequent analysis of SV shape characteristics in tissue that was immunostained for VGLUT1 and GlyT2. VGLUT1 immunostaining reliably and consistently marked terminals with round SVs and asymmetric PSDs (Fig. 3), in sharp contrast to unstained terminals in the same tissue. GlyT2 immunostaining consistently labeled terminals with pleomorphic SVs and symmetric PSDs (Fig. 4), and their appearance resembled those of VGLUT1-negative endings. Unstained terminals in the GlyT2-stained tissue resembled those immunostained by VGLUT1. Table 2 shows representative area and roundness values for the analyzed SVs of cats under

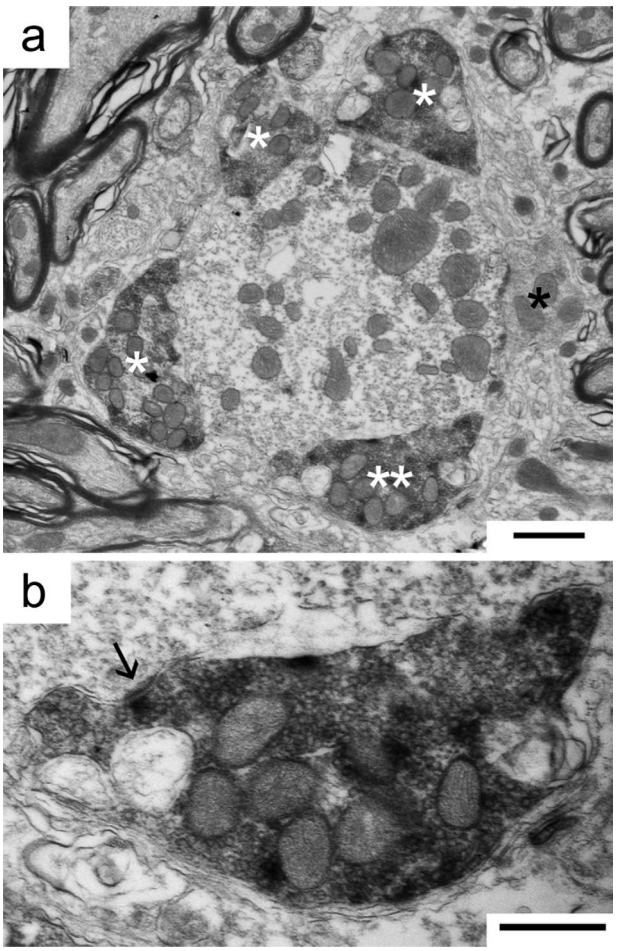

Figure 3. Immunohistochemical labeling of synaptic endings using VGLUT1 antibodies identifies excitatory synaptic contacts on an MSO dendrite of a cat with normal hearing. **a:** Cross-section through a dendrite shows four labeled endings (white asterisks) and one unlabeled ending (black asterisk). One labeled ending (double asterisks) is magnified in panel **b**, where an asymmetric postsynaptic density (arrow) and round SVs are consistent with the ending's inferred excitatory nature. Scale bars = 2 μm in a; 500 nm in b.

different fixation conditions. Note that tissues prepared under the same fixative conditions have similar roundness values for large round and small round vesicles. Tissues fixed with 2% glutaraldehyde/2% paraformaldehyde have larger roundness values than tissue fixed with 4% paraformaldehyde/0.1% glutaraldehyde. This finding is consistent with the literature and also highlights the importance of comparing SV shape and size within individual animals, minimizing variance due to fixation parameters.

Immunohistochemical staining of MSO tissue revealed that synaptic vesicles in endings positively labeled for VGLUT1 had roundness values (0.836 ± 0.26) commensurate with those classified as large round by morphometric analysis (0.803 ± 0.35). These data argue that endings with large round SVs are indeed excitatory in

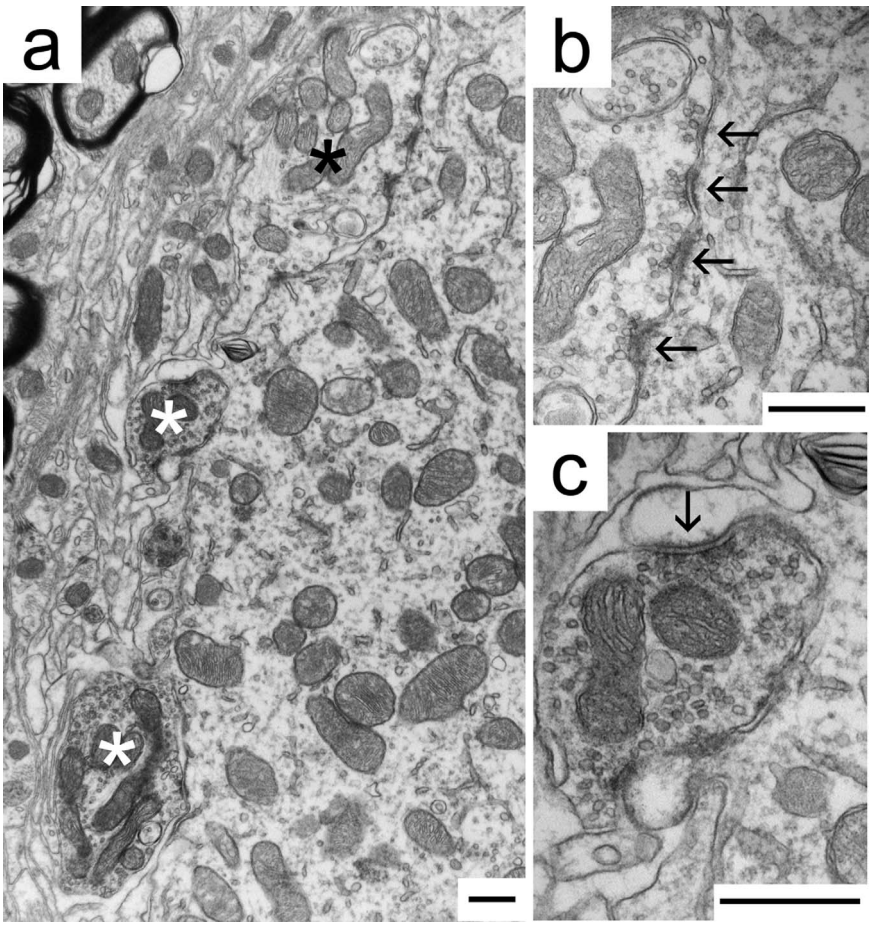

Figure 4. Immunohistochemical labeling of synaptic endings using GlyT2 antibodies identifies inhibitory synaptic contacts (white asterisks, **c**) on a representative MSO cell body of a cat with normal hearing (**a**). The immunoprecipitate darkens the mitochondria and forms a thin, dark halo around SVs, clearly revealing unstained terminals (black asterisk, **b**). b: A typical GlyT2-immunonegative ending has round SVs and asymmetric postsynaptic densities (arrows) characteristic of excitatory synapses. c: A typical GlyT2-immunopositive terminal has pleomorphic SVs and symmetric postsynaptic densities (arrow), characteristic of inhibitory synapses. Scale bars = 500 nm.

TABLE 2.
Fixation Type and Synaptic Vesicle Characteristics

Animal	Fixation type[1]	SV type	Number of terminals	Number of SVs	Area (ηm^2)	Roundness
Deaf 03-033	2%, 2%	LR	12	556	1964±130	0.833±0.033
		SR	4	166	1632±76	0.830±0.016
		PL	8	652	1720±244	0.724±0.020
Deaf 04-109	2%, 2%	LR	18	654	1774±114	0.837±0.035
		SR	8	378	1628±85	0.813±0.032
		PL	9	514	1615±97	0.721±0.018
Hearing 99-367	2%, 2%	LR	25	2516	1795±162	0.813±0.030
		SR	0	0	–	–
		PL	13	763	1760±200	0.709±0.034
Hearing 03-139	4%, 0.1%	LR	20	2368	1897±110	0.767±0.028
		SR	8	950	1670±88	0.761±0.019
		PL	22	1732	1763±120	0.706±0.042
Hearing 07-006	4%, 0.1%	LR	9	749	1822±75	0.766±0.116
		SR	6	756	1609±71	0.767±0.024
		PL	14	1531	1555±137	0.703±0.054

[1]% paraformaldehyde, % glutaraldehyde; SV, synaptic vesicle; LR, large round; SR, small round; PL, pleomorphic.

nature. A similar comparison equated the mean roundness of GlyT2-labeled SVs (0.713 ± 0.004) with the pleomorphic SVs identified using morphometric analysis (0.712 ± 0.009; Table 3). There are significant differences between the size and shape of excitatory and inhibitory SVs ($P < 0.05$, Tukey–Kramer HSD).

TABLE 3.
Immunohistochemistry and Synaptic Vesicle Characteristics

Animal	Fixation type	Immunolabeled	Number of terminals	Number of SVs	Area	Roundness
Hearing 08-022	4%, 0.1%	VGLUT1 Positive	13	1788	1660±345	0.806±0.084
		VGLUT1 Negative	7	730	1503±332	0.715±0.079
BCIK1	4%, 0.1%	VGLUT1 Positive	7	1050	1818±323	0.850±0.091
		VGLUT1 Negative	4	497	1172±227	0.708±0.112
BCIK1	4%, 0.1%	GlyT2 Positive	8	939	1436±318	0.715±0.132
		GlyT2 Negative	7	510	1618±397	0.851±0.091

SV, synaptic vesicle; BCIK, bilateral cochlear implant cat.

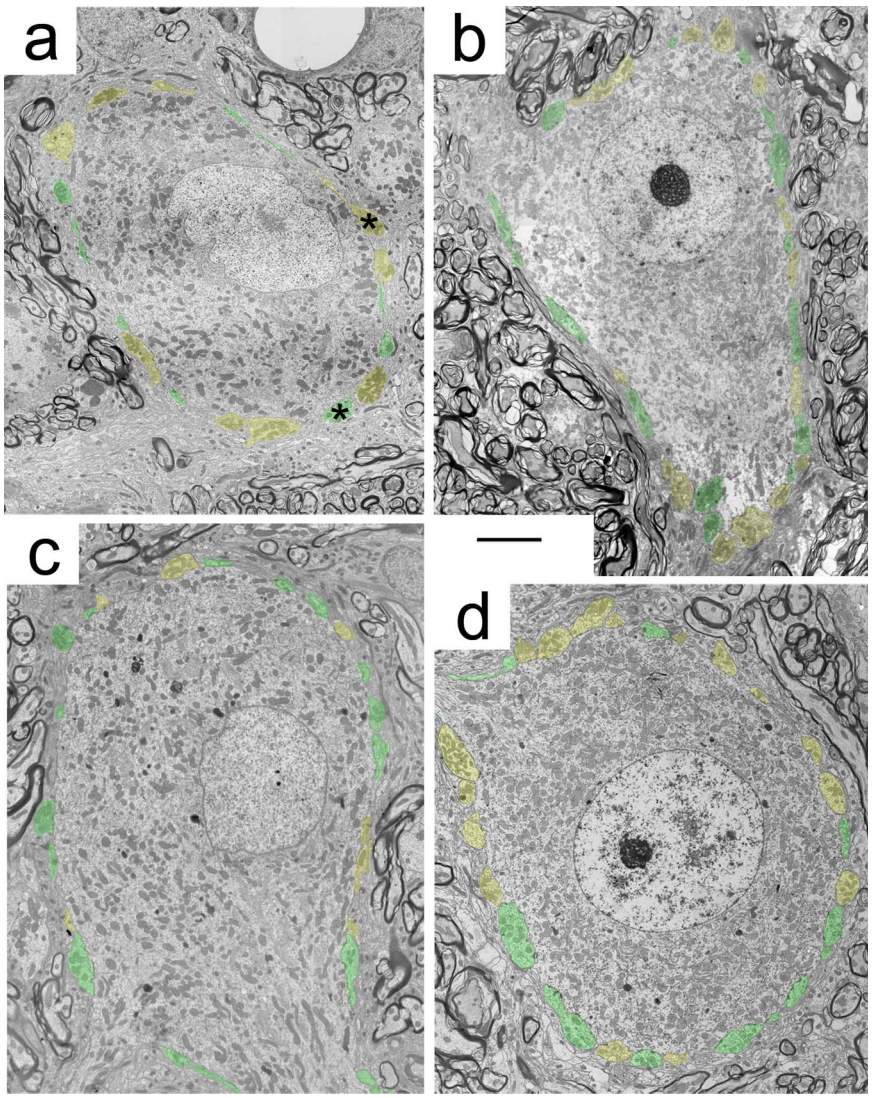

Figure 5. Representative electron micrographs of MSO principal cells from (**a**) a normal hearing cat, (**b**) a unilateral cochlear-implanted deaf cat, (**c**) an unstimulated congenitally deaf cat, and (**d**) a bilateral cochlear-implanted deaf cat. Inhibitory endings contain pleomorphic SVs and are highlighted in red, whereas excitatory endings contain small or large round SV and are highlighted in green. The representation of inhibitory axosomatic terminals diminishes with deafness, and is restored with stimulation through cochlear implants. Asterisks identify endings magnified in Figure 6. Scale bar = 5 μm.

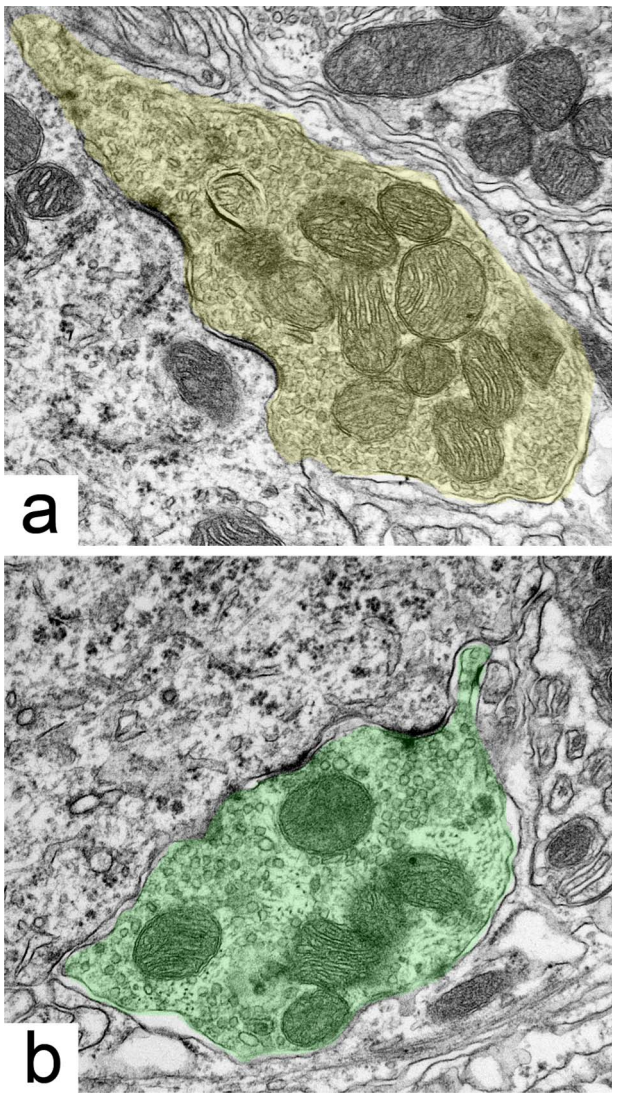

Figure 6. Representative electron micrographs of inhibitory (a) and excitatory (b) axosomatic terminals in the normal MSO, magnified from Figure 5a. Symmetric postsynaptic densities and pleomorphic synaptic vesicles indicate the ending is inhibitory (a), whereas asymmetric postsynaptic densities and round synaptic vesicles indicate the ending is excitatory (b). These structural features were used to classify endings as shown in Figure 5.

TABLE 4.

Axosomatic Inhibition on MSO Principal Cells

Cat I.D.	Total endings	Inhibitory	Excitatory	Percent inhibitory
DWC 03-033	22	7	15	31.82
DWC 04-109	27	8	19	29.63
DWC 04-109	12	3	9	25.00
DWC 04-109	27	9	18	33.33
DWC 98-354	23	7	16	30.43
DWC 07-047	16	4	12	25.00
DWC 03-033	16	5	11	31.25
DWK-90	39	10	29	25.64
DWK-90	28	8	20	28.57
DWK-90	18	5	13	27.78
DWK-90	33	6	27	18.18
Normal 99-367	30	16	14	53.33
Normal 07-006	20	10	10	50.00
Normal 07-006	28	13	15	46.43
Normal 07-006	16	7	9	43.75
Normal 03-139	41	21	20	51.22
Normal 03-139	26	11	15	42.31
PK-90	22	10	12	45.45
PK-90	21	12	9	57.14
PK-90	29	17	12	58.62
PK-90	19	10	9	52.63
CIK-2	7	3	4	42.86
CIK-2	45	27	18	60.00
CIK-2	39	15	24	38.46
CIK-3	29	17	12	58.62
CIK-3	13	7	6	53.84
CIK-3	22	10	12	45.45
CIK-3	42	21	21	50.00
CIK-8	19	9	10	47.37
CIK-8	20	10	10	50.00
CIK-8	21	9	12	42.86
CIK-8	19	8	11	42.10
CIK-8	19	10	9	52.63
BCIK-1	23	12	11	52.17
BCIK-1	14	9	5	64.28
BCIK-1	12	5	7	41.67
BCIK-1	29	18	11	62.06
BCIK-1	24	12	12	50.00
BCIK-1	34	13	21	38.24
BCIK-1	27	13	14	48.15
BCIK-1	35	16	19	45.71
BCIK-1	30	15	15	50.00
BCIK-3	14	7	7	50.00
BCIK-3	20	11	9	55.00
BCIK-3	17	8	9	47.06

Each row represents the analysis from a single cell. DWC, deaf white cat with ID number; DWK-90. 90-day-old deaf white cat; Normal, normal hearing cat with ID number; PK-90, 90-day-old hearing, pigmented cat; CIK-2, -3, and -8, unilateral cochlear implant cats; BCIK-1, -3, bilateral cochlear implant cats.

Axosomatic contacts on MSO principal cells

Our analysis of synaptic inputs to the MSO principal cell body confirmed that the somata are studded with endings, most of which appear as small boutons with either excitatory or inhibitory characteristics as illustrated by electron micrographs of representative cell bodies from each cohort (Fig. 5). The inhibitory synapses exhibit pleomorphic SVs that face relatively symmetric membrane thickenings (Fig. 6a), whereas excitatory synapses have round SVs that face asymmetric membrane thickenings (Fig. 6b). Although analysis revealed no difference in the average total number of axosomatic terminations for all cohorts (mean range 20.4–29.5), there was a clear difference in number of inhibitory synapses between the deaf, hearing, and cochlear-implanted animals (Table 4). Inhibitory inputs are more prevalent on MSO cell bodies of hearing (12.7 $\pm$ 4.2, $n = 10$), unilateral cochlear-implanted cats (CIK, 12.2 $\pm$ 6.7, $n = 12$), and bilateral cochlear-implanted cats (BCIK, 11.6 $\pm$ 3.8, $n = 12$). In contrast, there are significantly smaller numbers of

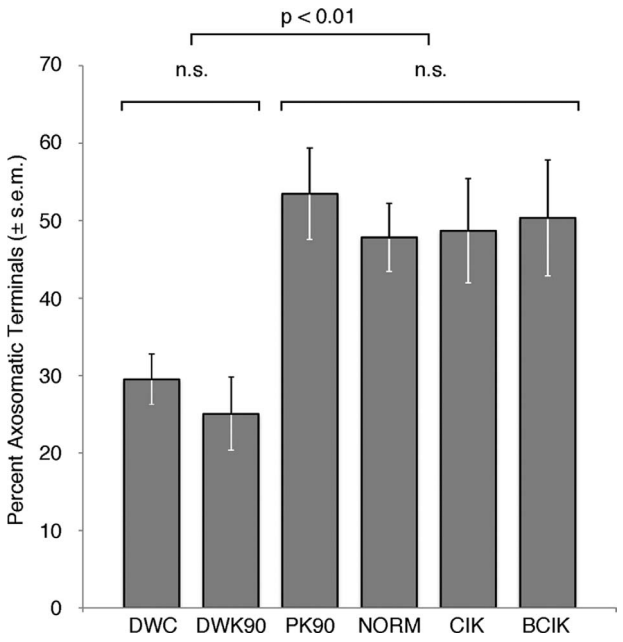

Figure 7. The proportion of inhibitory axosomatic terminals is shown for all animals, grouped by cohort. Deaf cats have significantly smaller percentage of inhibitory contacts (DWC and DWK90; 27.9 ± 4.3%, $n = 11$) than hearing (PK90 and NORM; 50.1 ± 5.5%, $n = 10$) or cochlear-implanted animals (CIK and BCIK; 49.5 ± 7.0, $n = 24$; one-way ANOVA, $P < 0.0001$).

inhibitory inputs to MSO cell bodies of unstimulated congenitally deaf cats (6.5 ± 2.2, $n = 11$; one-way analysis of variance [ANOVA], $P = 0.0164$). Additionally, we show that at the age of implantation the MSO of deaf kittens have fewer inhibitory synapses on principal cell bodies (7.3 ± 2.2, $n = 4$) compared with the hearing kitten (PK; 12.3 ± 3.3, $n = 4$), suggesting that cochlear implant stimulation restores inhibition on the soma (Student's *t*-test, $P = 0.0229$). Excitatory inputs are present on the soma, but there is no statistically significant difference in the number of excitatory contacts when comparing hearing (12.5 ± 3.6, $n = 10$), deaf (17.2 ± 6.4, $n = 11$), CIK (12.4 ± 5.8, $n = 12$), and BCIK (11.7 ± 4.9, $n = 12$; one-way ANOVA, $P = 0.3829$). The proportion of inhibitory axosomatic inputs is graphically illustrated (Fig. 7); deaf animals have a significantly smaller proportion of inhibitory endings (27.9 ± 4.3%, $n = 11$) than hearing (50.1 ± 5.5%, $n = 10$) or cochlear-implanted animals (CIK, 48.7 ± 6.7%, $n = 12$; BCIK, 50.4 ± 7.5, $n = 12$), which have similar proportions (one-way ANOVA, $P < 0.0001$). The proportion of inhibitory inputs of deaf kittens (DWK90; 53.4 ± 5.9%, $n = 4$) and hearing kittens (PK90; 25.0 ± 4.7%, $n = 4$) were similar to the adult deaf and adult hearing cats, respectively.

Axodendritic contacts on MSO principal cells

The dendrites of the principal cells are marked by the presence of numerous bouton endings. The inferred strength of excitatory inputs to the MSO cell dendrites was quantified by measuring the size of VGLUT1-positive boutons in hearing, deaf, and cochlear-implanted deaf cats. While the density of the boutons does not change along the length of dendrites when comparing between cohorts, the size of the boutons does. Hearing cats had the largest average endings (2.346 ± 1.356 μm^2, $n = 945$), whereas deaf cats had significantly smaller ones (1.309 ± 0.674 μm^2, $n = 286$). After ≈3 months of stimulation, excitatory boutons (1.932 ± 1.0873 μm^2, $n = 810$) were larger on average than those in deaf cats, but smaller than those in hearing cats (one-way ANOVA, $P < 0.0001$). Photomicrographs show VGLUT1-labeled boutons on the dendrites of hearing, deaf, and deaf-implanted cats; mean bouton size in hearing cats is clearly larger than that of deaf cats, whereas the cochlear-implanted cat has endings that are intermediate in size (Fig. 8).

Synaptic vesicle analysis of axodendritic terminals also revealed a change in the proportion of excitatory and inhibitory inputs along the dendrites. Most terminals from each of the cohorts exhibited the morphology of excitatory synapses with a prominent postsynaptic density and round synaptic vesicles (Fig. 3). SV analysis revealed that there were no endings with inhibitory features observed along the dendrites of congenitally deaf cats. In contrast, the proportion of endings with inhibitory features was 28.3 ± 12.8% in normal-hearing cats and 24.8 ± 11.5% in cochlear-implanted cats. The restoration of inhibition for implanted cats was statistically significant ($P < 0.0001$, Tukey–Kramer HSD) compared with that of deaf cats. There was no difference between hearing and cochlear-implanted cats.

These results, as well as those from the axosomatic analysis, are summarized in Figure 9. Normal-hearing cats exhibit a specific pattern of axosomatic inhibition and axodendritic excitation, which is disrupted in congenitally deaf cats. Cochlear implant stimulation is able to restore the pattern of excitation and inhibition in the deaf MSO to a more normal state.

MSO cell body size and synapse density

Other measured qualities of the somatic analysis included the cross-sectional perimeter and area of the MSO principal cell bodies. There were no significant differences among hearing (103.0 ± 17.1 μm; 515.1 ± 66.9 μm^2, $n = 8$), deaf (98.5 ± 9.6 μm; 562.4 ± 101.1 μm^2, $n = 10$), or cochlear-implanted animals (97.0 ± 19.6 μm; 510.0 ± 165.2 μm^2, $n = 21$) for any of these measures (one-way ANOVA, $P = 0.3288$, $P = 0.7732$).

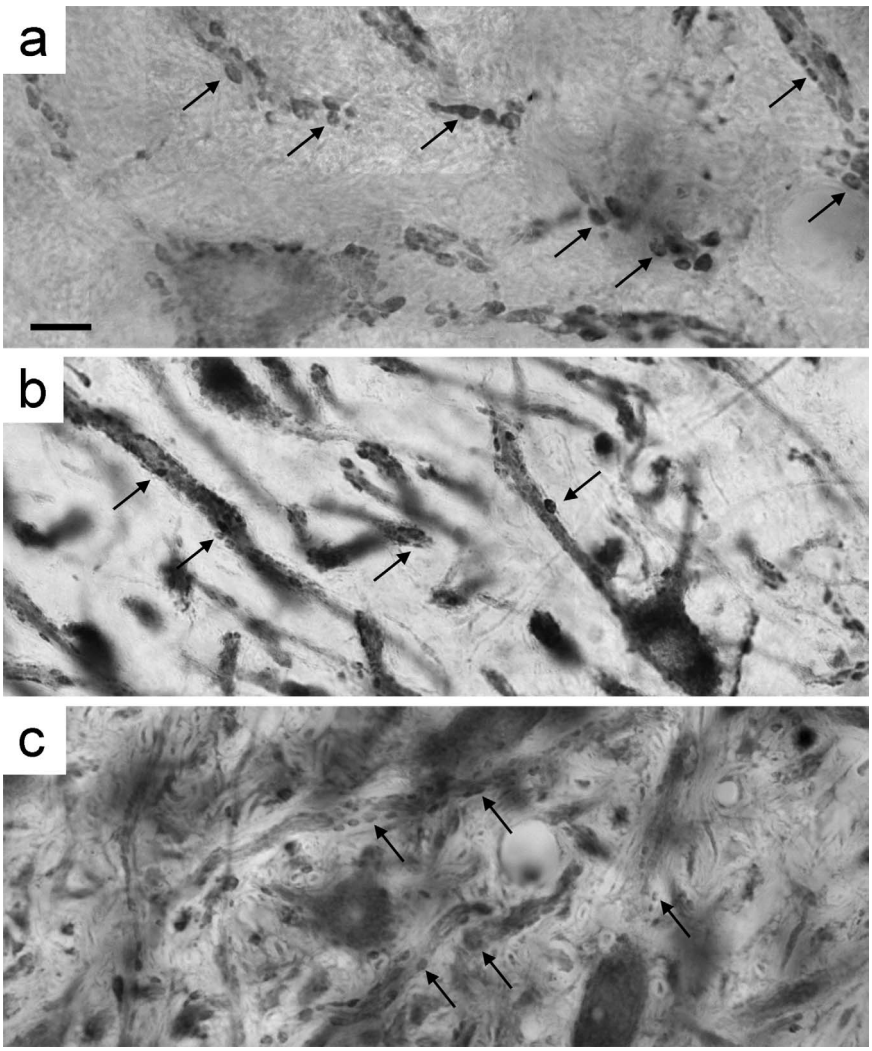

Figure 8. Light micrographs of VGLUT1 immunohistochemical-stained tissue show variations in the size of axodendritic endings in the MSO between hearing (**a**), deaf (**b**), and cochlear-implant stimulated (**c**) cats. Mean bouton size in hearing cats was largest, while the mean bouton size of deaf cats was statistically smallest among the cohorts. The mean bouton size of cochlear-implant stimulated cats was significantly different from deaf or hearing cats, and of an intermediate size. Arrows in each panel indicate a few examples of VGLUT1-positive boutons. Scale bar = 10 μm.

The density of synapses on the MSO soma, defined as the number of synapses per unit length of soma perimeter, also did not show statistically significant differences between the cohorts: hearing (0.217 ± 0.017 endings/μm, $n = 8$), deaf (0.251 ± 0.065 endings/μm, $n = 9$), and cochlear-implanted (0.249 ± 0.080 endings/μm, $n = 22$; one-way ANOVA, $P = 0.3217$).

DISCUSSION

In the present study, analysis of synaptic endings on the somata of MSO cells in hearing, deaf, and cochlear-implanted cats show that activation of the auditory system via cochlear implant stimulation alters the synaptic organization of MSO principal cells in congenitally deaf cats. We observed a significant increase in the number of inhibitory inputs in the MSO after ≈3 months of cochlear implant stimulation when compared with deaf animals with no implants. This restoration of inhibitory inputs caused the MSO of cochlear-implanted cats to appear statistically similar to that of the MSO of normal-hearing cats. Additionally, analysis of somatic inputs to 3-month-old kittens showed that at the time of implantation the deaf kittens already had significantly fewer inhibitory axosomatic inputs than normal-hearing kittens. Finally, we showed that the axodendritic excitatory inputs to the MSO dendrites are smaller in deaf animals than in hearing, and that unilateral and bilateral cochlear implant stimulation increases the excitatory bouton size. Taken together, these results show that electrical stimulation

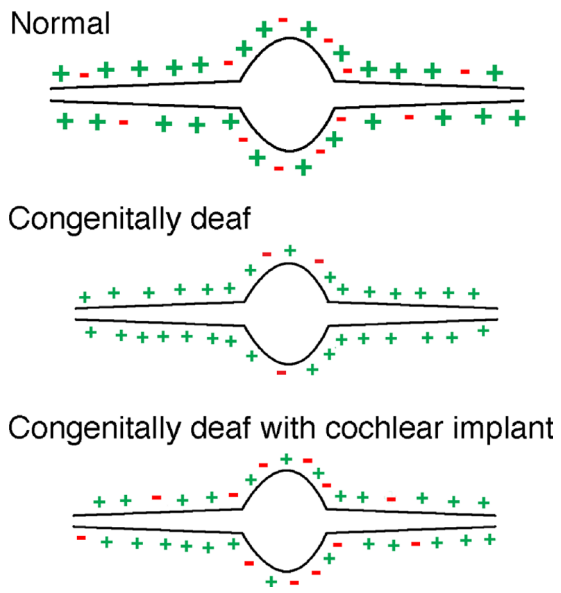

Figure 9. Schematic summary of the distribution and size of input terminals to the principal cells of the MSO. In normal-hearing cats there is approximately an even split of excitatory and inhibitory terminals on the cell body with mostly excitatory inputs to the dendrites. With congenital deafness, the size of the terminals shrinks and the relative number of inhibitory terminals is reduced on the cell body and vanishes on the dendrites. The introduction of activity to the auditory system via cochlear implants restores the distribution of inhibitory terminals to the neurons and partially restores terminal size.

through cochlear implants exerts a powerful effect on the balance of inhibition and excitation in this binaural auditory nucleus.

Analysis of synaptic vesicle morphology

Structural analysis of SVs has been used as a tool to characterize synaptic junctions. While it is known that all synaptic vesicles are spherical in situ (Tatsuoka and Reese, 1989), an interaction between aldehydes and SVs during fixation results in a fortuitous artifact—a flattening of the SVs of inhibitory endings (Uchizono, 1965; Larramendi et al., 1967; Bodian, 1970; Atwood and Lang, 1972). The extent of SV flattening has been attributed to a number of fixation variables, including differing concentrations of glutaraldehyde (Tisdale and Nakajima, 1976). The PSD is less affected by the fixation method, and when visible can be used to distinguish synapse type (Tisdale and Nakajima, 1976; Uchizono, 1965). PSDs, however, can be blurred, unclear, or absent from the section being examined, leaving SV shape as the primary tool to determine synapse type. The classification of SV shape has previously been subjective and inconsistent; some studies identify three types of SVs (Cant and Morest, 1979), whereas others have described four types (Helfert et al., 1992) or more (Munirathinam et al., 2004; Gomez-Nieto and Rubio, 2009).

While the method of SV analysis presented here is unique in certain aspects, it is based on traditional methods for ultrastructure analysis. Our approach, however, takes advantage of the underlying connection between structure and function, and combines two powerful histological methods—immunohistochemistry and electron microscopy—to complement and validate each other. Previous studies have qualitatively observed SV shape and size; however, none have employed such a quantitative approach to studying the vesicle attributes. Digital image analysis of precisely drawn SV outlines provides numerical measures for size and roundness. A vesicle that might have previously been labeled “large round” is now categorized as such by measurable characteristics, to which statistical tests can be applied. Additionally, when analyzing SVs from multiple synapses, the absolute values for SV area and roundness are considered relative to other synapses in the same animal. As a result, variations in fixation parameters did not have an effect when discerning between synapse types in these studies.

We identified three distinct types of synaptic vesicles consistent with those reported in the literature: large round, small round, and pleomorphic. It is generally accepted that round SVs are found in excitatory synapses, which was consistent with our VGLUT1 staining. The calculated roundness and area measures of SVs in the labeled synapses indicate that these are large round vesicles. Synapses with pleomorphic vesicles were singularly stained by antibodies against GlyT2 and positively identified. In the context of numerous reports from the literature, we are confident in defining inhibitory and excitatory inputs to the MSO cell body by studying the synaptic ultrastructure.

We acknowledge that there are alternative methods for characterizing synaptic behavior, but none were appropriate for this study. In vivo electrophysiological recordings were not practical due to the age of our animals after implantation and stimulation. Moreover, in vivo recordings would be extremely challenging not only because of the electrical artifact from stimulation via the cochlear implant but also because of the inherent difficulty in experimentation of the MSO (e.g., Guinan et al., 1972; Brownell, 1975; Spirou et al., 1990). A few groups have been able to successfully record the neuronal activity of principal cells in the MSO region but success has been low (Kapfer et al., 2002).

Inhibition to the medial superior olive

While the exact mechanisms for processing ITD cues has yet to be unraveled, inhibition in the MSO is critical to a functional hearing animal (Brand et al., 2002; Grothe,

2003; Pecka et al., 2007, 2008). Neuronal tract tracing studies have shown that the excitatory endings from the anteroventral cochlear nucleus are distributed along the lateral dendrites of the ipsilateral MSO and along the medial dendrites of the contralateral MSO (Stotler, 1953; Clark, 1969a,b; Perkins, 1973; Cant and Casseday, 1986; Casseday et al., 1988; Schofield and Cant, 1991). MSO principal cells also receive axosomatic inhibitory inputs ipsilaterally from the LNTB and contralaterally from the MNTB (Kuwabara and Zook, 1992; Grothe and Sanes, 1993; Magnusson et al., 2005; Hassfurth et al., 2010). The inhibitory endings are found consistently in species with low-frequency hearing, including the cat (Clark 1969a,b), chinchilla (Perkins, 1973), gerbil (Cant and Hyson, 1992), and guinea pig (Helfert et al., 1989). Cochlear ablation studies in the gerbil (Kapfer et al., 2002; Russell and Moore, 2002) have further shown that normal development of MSO inhibition is experience-dependent, implicating the importance of inhibition in ITD detection.

We observed statistically significantly changes in the proportion of inhibitory endings in the MSO of cats after a period of cochlear implant stimulation. Although hearing and congenitally deaf cats had a similar total number of endings on MSO somata, there was a decrease in inhibitory endings to 27.9% in congenitally deaf cats compared with 50.1% in hearing cats. After a 2–3-month period of unilateral or bilateral stimulation of the auditory nerve via cochlear implants in congenitally deaf cats, the percentage of inhibitory endings on MSO somata was 49.5%, approximately equal to that of normal-hearing animals. A statistical analysis of the three cohorts showed that normal-hearing and cochlear-implanted animals had a statistically similar proportion of inhibitory inputs, and both of these groups of animals had a significantly higher proportion of inhibitory inputs when compared with that of deaf animals. These results emphasize the experience-dependent importance for the synaptic organization of inhibition in the MSO.

We next asked if the higher proportion of inhibitory inputs were present in the deaf animal at the time of implantation. Such a result would inform us whether the inhibition was restored or simply maintained by the cochlear implant simulation. Two 3-month-old kittens were analyzed with respect to inputs to the MSO. The proportion of inhibitory endings on the somata of the hearing kitten was 53.5% inhibition, whereas the proportion for the deaf kittens was 25.0%. Thus, we conclude that at the time of implantation, deaf kittens have a level of MSO inhibition less than that of age-matched hearing kittens, and that cochlear implant stimulation is able to restore MSO somatic inhibition to a level similar to that of an adult hearing cat.

Excitation to the medial superior olive

Excitation of bilateral dendrites in the mammalian MSO is critical for successful ITD detection. Excitatory inputs to the MSO project from the ipsilateral and contralateral VCN, and the relationship between these connections and ITD detection have been a focus of study for decades. Early models theorized that the MSO neuron is a coincidence detector, receiving phase-locked input from both cochlear nuclei on respective bilateral dendrites, which were arranged as varying delay lines (Jeffress 1948). While recent work indicates that somatic inhibition also plays an important role in the timing of dendritic inputs (Smith et al., 1993; Zhou et al., 2005; Pecka et al., 2008; Werthat et al., 2008; Drapal and Marsalek, 2011), dendritic excitation is certainly a key in ITD detection. In our study, 3 months of cochlear implant stimulation seemed to partially restore the size of axodendritic excitatory boutons. Our analysis of dendritic excitation in the MSO revealed that the average size of synaptic boutons is smaller in congenitally deaf cats than in aged-matched hearing cats. Electrical stimulation of the auditory system via cochlear implants resulted in an increase in the size of boutons. Although these were still smaller than those in the normal-hearing cat, the partial size increase could represent a stimulation-driven increase in synaptic strength of VCN projections to the MSO. It is tempting to speculate that continued stimulation could continue to restore terminal size toward normal.

Medial superior olive plasticity and cochlear implant stimulation

This study raises a number of questions concerning stimulation and plasticity in the auditory pathway. It has been generally accepted that there is a critical period of synaptic plasticity that ends well before adolescence. From our work, it appears as though this period of plasticity extends to at least the third and fourth months of kittens' development. The question that remains to be answered is how long and to what degree this plasticity remains in effect. Additionally, plasticity in only one region of the MSO was considered in this study. We analyzed MSO cells only in the ventral third of the nucleus, or the high-frequency processing region, which correlated with the region of the cochlea stimulated by the cochlear implants. It seems important to assess synaptic changes in the low-frequency regions of the MSO where most ITD processing is assumed to occur.

Our results have direct relevance to cochlear implant use in humans. Cochlear implant users have difficulty localizing sounds, and distinguishing a target sound in a noisy environment. Both of these hearing abilities are dependent on successful detection of ITDs. Recent work

examining ITD detection between congenitally deaf white cats and acutely deafened normal cats has shown significant differences in ITD sensitivity in the inferior colliculus (Hancock et al., 2010). When stimulated via cochlear implant, congenitally deaf cats had half as many ITD-sensitive neurons in the inferior colliculus as compared with deafened cats with previously normal hearing. Those neurons that were ITD-sensitive were more broadly tuned and had variable best ITD frequencies. The authors concluded that the precision of ITD detection is dependent on auditory experience, potentially through experience-driven refinement of the auditory circuits. IC neurons of congenitally deaf animals exhibited much greater levels of spontaneous activity, which might also reflect a "release of inhibition" due to the reduced proportion of inhibitory inputs to MSO neurons. We predict that IC units in cochlear-implanted cats would exhibit low levels of spontaneous discharges as found in normal-hearing cats. Our work with congenitally deaf cats indicates that cochlear implant stimulation can restore auditory structures to a more normal state when the animals were implanted at 3 months.

In conclusion, this study contributes to the growing evidence that demonstrates profound plasticity in the mammalian auditory system. Auditory neurons react quickly and pathologically to the lack of acoustic input (West and Harrison, 1973; Schwartz and Higa, 1982; Kral et al., 2002; Baker et al., 2010), which alters the synaptic organization of MSO principal cells in congenitally deaf cats. Perhaps most remarkable is the extent to which plasticity of synapse morphology and organization occurs when neuronal activity is restored in the auditory system. The plasticity observed in the MSO implies that true bilateral cochlear implants could potentially restore sound localization circuits that would significantly enhance sound localization and speech discrimination in noise for human users.

ACKNOWLEDGMENTS

The authors thank Tan Pongstaporn for assistance with electron microscopy, Christa Baker for immunohistochemical procedures, Jahn O'Neil and Karen Montey for animal training, and Charles Limb for surgical assistance.

LITERATURE CITED

Atwood HL, Lang F, Morin WA. 1972. Synaptic vesicles: selective depletion in crayfish excitatory and inhibitory axons. Science 176:1353–1355.

Babalian AL, Ryugo DK, Rouiller EM. 2003. Discharge properties of identified cochlear nucleus neurons and auditory nerve fibers in response to repetitive electrical stimulation of the auditory nerve. Exp Brain Res 153:452–460.

Baker CA, Montey KL, Pongstaporn T, Ryugo DK. 2010. Postnatal development of the endbulb of held in congenitally deaf cats. Front Neuroanat 4:19.

Barrett TW. 1976. Superposition of binaural influences on single neuron activity in the medial superior olive elicited by electrical stimulation of the osseous spiral laminae. Brain Res Bull 1:209–228.

Bodian D. 1970. An electron microscopic characterization of classes of synaptic vesicles by means of controlled aldehyde fixation. J Cell Biol 44:115–124.

Bourk TR. 1976. Electrical responses of neural units in the anteroventral cochlear nucleus of the cat. PhD Dissertation. Cambridge, MA: Massachusetts Institute of Technology.

Brand A, Behrend O, Marquardt T, McAlpine D, Grothe B. 2002. Precise inhibition is essential for microsecond interaural time difference coding. Nature 417:543–547.

Brownell WE. 1975. Organization of the cat trapezoid body and the discharge characteristics of its fibers. Brain Res 94:413–433.

Cant NB, Casseday JH. 1986. Projections from the anteroventral cochlear nucleus to the lateral and medial superior olivary nuclei. J Comp Neurol 247:457–476.

Cant NB, Hyson RL. 1992. Projections from the lateral nucleus of the trapezoid body to the medial superior olivary nucleus in the gerbil. Hear Res 58:26–34.

Cant NB, Morest DK. 1979. The bushy cells in the anteroventral cochlear nucleus of the cat. A study with the electron microscope. Neuroscience 4:1925–1945.

Cant NB, Morest DK. 1984. The structural basis for stimulus coding in the cochlear nucleus of the cat. In: Berlin CI, editor. Hearing science, recent advances. San Diego: College-Hill Press. p 371–421.

Casseday JH, Covey E, Vater M. 1988. Connections of the superior olivary complex in the rufous horseshoe bat Rhinolophus rouxi. J Comp Neurol 278:313–329.

Chao TK, Burgess BJ, Eddington DK, Nadol JB Jr. 2002. Morphometric changes in the cochlear nucleus in patients who had undergone cochlear implantation for bilateral profound deafness. Hear Res 174:196–205.

Chen I, Limb CJ, Ryugo DK. 2010. The effect of cochlear implant-mediated electrical stimulation on spiral ganglion cells in congenitally deaf white cats. JARO 11:587–603.

Clark GM. 1969a. Vesicle shape versus type of synapse in the nerve endings of the cat medial superior olive. Brain Res 15:548–551.

Clark GM. 1969b. The ultrastructure of nerve endings in the medial superior olive of the cat. Brain Res 14:293–305.

Drapal M, Marsalek P. 2011. Stochastic model explains role of excitation and inhibition in binaural sound localization in mammals. Physiol Res 60:573–583.

Dunn CC, Yost W, Noble WG, Tyler RS, Witt SA. 2006. Advantages of binaural hearing. In: Waltzman SB, Roland JR Jr, editors. Cochlear implants, 2nd ed. New York: Thieme Medical Publishers. p 205–213.

Elverland HH, Mair IW. 1980. Hereditary deafness in the cat. An electron microscopic study of the spiral ganglion. Acta Otolaryngol 90:360–369.

Friauf E, Aragón C, Löhrke S, Westenfelder B, Zafra F. 1999. Developmental expression of the glycine transporter GLYT2 in the auditory system of rats suggests involvement in synapse maturation. J Comp Neurol 412:17–37.

Gomez-Nieto R, Rubio ME. 2009. A bushy cell network in the rat ventral cochlear nucleus. J Comp Neurol 516: 241–263.

Grothe B. 1994. Interaction of excitation and inhibition in processing of pure tone and amplitude-modulated stimuli in the medial superior olive of the mustached bat. J Neurophysiol 71:706–721.

Grothe B. 2000. The evolution of temporal processing in the medial superior olive, an auditory brainstem structure. Prog Neurobiol 61:581–610.

Grothe B. 2003. New roles for synaptic inhibition in sound localization. Nat Rev Neurosci 4:540–550.

Grothe B, Sanes DH. 1993. Bilateral inhibition by glycinergic afferents in the medial superior olive. J Neurophysiol 69: 1192–1196.

Guinan JJ Jr, Norris BE, Guinan SS. 1972. Single auditory units in the superior olivary complex. II: Locations of unit categories and tonotopic organization. Int J Neruosci 4:147–166.

Hancock KE, Noel V, Ryugo DK, Delgutte B. 2010. Neural coding of interaural time differences with bilateral cochlear implants: effects of congenital deafness. J Neurosci 30: 14068–14079.

Hassfurth B, Grothe B, Koch U. 2010. The mammalian interaural time difference detection circuit is differentially controlled by GABAB receptors during development. J Neurosci 30:9715–9727.

Heid S, Hartmann R, Klinke R. 1998. A model for prelingual deafness, the congenitally deaf white cat—population statistics and degenerative changes. Hear Res 115:101–112.

Helfert RH, Bonneau JM, Wenthold RJ, Altschuler RA. 1989. GABA and glycine immunoreactivity in the guinea pig superior olivary complex. Brain Res 501:269–289.

Helfert RH, Juiz JM, Bledsoe SCJ, Bonneau JM, Wenthold RJ, Altschuler RA. 1992. Patterns of glutamate, glycine, and GABA immunolabeling in four synaptic terminal classes in the lateral superior olive of the guinea pig. J Comp Neurol 323:305–325.

Jeffress LA. 1948. A place theory of sound localization. J Comp Physiol Psych 41:35–39.

Kapfer C, Seidl AH, Schweizer H, Grothe B. 2002. Experience-dependent refinement of inhibitory inputs to auditory coincidence-detector neurons. Nat Neurosci 5:247–253.

Klinke R, Kral A, Heid S, Tillein J, Hartmann R. 1999. Recruitment of the auditory cortex in congenitally deaf cats by long-term cochlear electrostimulation. Science 285: 1729–1733.

Kral A, Hartmann R, Tillein J, Heid S, Klinke R. 2002. Hearing after congenital deafness: central auditory plasticity and sensory deprivation. Cereb Cortex 12:797–807.

Kral A, Tillein J, Heid S, Hartmann R, Klinke R. 2005. Postnatal cortical development in congenital auditory deprivation. Cereb Cortex 15:552–562.

Kretzmer EA, Meltzer NE, Haenggeli CA, Ryugo DK. 2004. An animal model for cochlear implants. Arch Otolaryngol Head Neck Surg 130:499–508.

Kulesza RJ Jr. 2007. Cytoarchitecture of the human superior olivary complex: medial and lateral superior olive. Hear Res 225:80–90.

Kuwabara N, Zook JM. 1992. Projections to the medial superior olive from the medial and lateral nuclei of the trapezoid body in rodents and bats. J Comp Neurol 324: 522–538.

Larramendi LM, Fickenscher L, Lemkey-Johnston N. 1967. Synaptic vesicles of inhibitory and excitatory terminals in the cerebellum. Science 156:967–969.

Liberman MC. 1982. The cochlear frequency map for the cat: Labeling auditory-nerve fibers of known characteristic frequency. J Acoust Soc Am 75:1441–1449.

Lustig LR, Leake PA, Snyder RL, Rebscher SJ. 1994. Changes in the cat cochlear nucleus following neonatal deafening and chronic intracochlear electrical stimulation. Hear Res 74:29–37.

Magnusson AK, Kapfer C, Grothe B, Koch U. 2005. Maturation of glycinergic inhibition in the gerbil medial superior olive after hearing onset. J Physiol 568(Pt 2):497–512.

Mair IW. 1973. Hereditary deafness in the white cat. Acta Otolaryngol 314:1–48.

Matsushima J-I, Shepherd RK, Seldon HL, Xu S-A, Clark GM. 1991. Electrical stimulation of the auditory nerve in deaf kittens: effects on cochlear nucleus morphology. Hear Res 56:133–142.

Matthews G, Sterling P. 2008. Evidence that vesicles undergo compound fusion on the synaptic ribbon. J Neurosci 28: 5403–5411.

Munirathinam S, Ostapoff EM, Gross J, Kempe GS, Dutton JA, Morest DK. 2004. Organization of inhibitory feed-forward synapses from the dorsal to the ventral cochlear nucleus in the cat: a quantitative analysis of endings by vesicle morphology. Hear Res 198:99–115.

O'Neil JN, Limb CJ, Baker CA, Ryugo DK. 2010. Bilateral effects of unilateral cochlear implantation in congenitally deaf cats. J Comp Neurol 518:2382–2404.

Pecka M, Zahn TP, Saunier-Rebori B, Siveke I, Felmy F, Wiegrebe L, Klug A, Pollak GD, Grothe B. 2007. Inhibiting the inhibition: a neuronal network for sound localization in reverberant environments. J Neurosci 27:1782–1790.

Pecka M, Brand A, Behrend O, Grothe B. 2008. Interaural time difference processing in the mammalian medial superior olive: the role of glycinergic inhibition. J Neurosci 28: 6914–6925.

Perkins RE. 1973. An electron microscopic study of synaptic organization in the medial superior olive of normal and experimental chinchillas. J Comp Neurol 148:387–415.

Peters A, Palay SF, Webster Hd. 1991. The fine structure of the nervous system: neurons and their supporting cells. New York: Oxford University Press.

Petralia RS, Wang YX, Wenthold RJ. 2003. Internalization at glutamatergic synapses during development. Eur J Neurosci 18:3207–3217.

Russell FA, Moore DR. 2002. Ultrastructural transynaptic effects of unilateral cochlear ablation in the gerbil medial superior olive. Hear Res 173:43–61.

Ryugo DK, Pongstaporn T, Huchton DM, Niparko JK. 1997. Ultrastructural analysis of primary endings in deaf white cats: morphologic alterations in endbulbs of Held. J Comp Neurol 385:230–244.

Ryugo DK, Rosenbaum BT, Kim PJ, Niparko JK, Saada AA. 1998. Single unit recordings in the auditory nerve of congenitally deaf white cats: morphological correlates in the cochlea and cochlear nucleus. J Comp Neurol 397:532–548.

Ryugo DK, Cahill HB, Rose LS, Rosenbaum BT, Schroeder ME, Wright AL. 2003. Separate forms of pathology in the cochlea of congenitally deaf white cats. Hear Res 181:73–84.

Ryugo DK, Kretzmer EA, Niparko JK. 2005. Restoration of auditory nerve synapses in cats by cochlear implants. Science 310:1490–1492.

Scheibel ME, Scheibel AB. 1974. Neuropil organization in the superior olive of the cat. Exp Neurol 43:339–348.

Schikorski T, Stevens CF. 1997. Quantitative ultrastructural analysis of hippocampal excitatory synapses. J Neurosci 17:5858–5867.

Schofield BR, Cant NB. 1991. Organization of the superior olivary complex in the guinea pig. I. Cytoarchitecture, cytochrome oxidase histochemistry, and dendritic morphology. J Comp Neurol 314:645–670.

Schwartz IR, Higa JF. 1982. Correlated studies of the ear and brainstem in the deaf white cat: changes in the spiral ganglion and the medial superior olivary nucleus. Acta Otolaryngol 93:9–18.

Smith PH, Joris PX, Yin TC. 1993. Projections of physiologically characterized spherical bushy cell axons from the cochlear nucleus of the cat: Evidence for delay lines to the medial superior olive. J Comp Neurol 33:245–260.

Spirou GA, Brownell WE, Zidanic M. 1990. Recordings from cat trapezoid body and HRP labeling of globular bushy cell axons. J Neurophysiol 63:1169–1190.

Stotler WA. 1953. An experimental study of the cells and connections of the superior olivary complex of the cat. J Comp Neurol 98:401–432.

Tatsuoka H, Reese TS. 1989. New structural features of synapses in the anteroventral cochlear nucleus prepared by direct freezing and freeze-substitution. J Comp Neurol 290:343–357.

Tisdale AD, Nakajima Y. 1976. Fine structure of synaptic vesicles in two types of nerve terminals in crayfish stretch receptor organs: influence of fixation methods. J Comp Neurol 165:369–386.

Uchizono K. 1965. Characteristics of exitatory and inhibitory synapses in the central nervous systems of the cat. Nature 207:642–643.

van Hoesel RJ. 2004. Exploring the benefits of bilateral cochlear implants. Audiol Neurootol 9:234–246.

van Hoesel RJ. 2007. Sensitivity to binaural timing in bilateral cochlear implant users. J Acoust Soc Am 121: 2192–2206.

Werthat F, Alexandrova O, Grothe B, Koch U. 2008. Experience-dependent refinement of the inhibitory axons projecting to the medial superior olive. Dev Neurobiol 68: 1454–1562.

West CD, Harrison JM. 1973. Transneuronal cell atrophy in the deaf white cat. J Comp Neurol 151:377–398.

Zhou Y, Carney LH, Colburn HS. 2005. A model for interaural time difference sensitivity in the medial superior olive: interaction of excitatory and inhibitory synaptic inputs, channel dynamics, and cellular morphology. J Neurosci 25: 3046–3058.

Zhou J, Nannapaneni N, Shore S. 2007. Vessicular glutamate transporters 1 and 2 are differentially associated with auditory nerve and spinal trigeminal inputs to the cochlear nucleus. J Comp Neurol 500:777–787.